

Electron-phonon mechanism does not explain the photoemission kink in cuprate superconductors

Feliciano Giustino^{1,2}, Marvin L. Cohen^{1,2} & Steven G. Louie^{1,2}

¹*Department of Physics, University of California at Berkeley, California 94720, USA.*

²*Materials Sciences Division, Lawrence Berkeley National Laboratory, Berkeley, California 94720, USA.*

Despite over two decades of intense research efforts, the origin of high-temperature superconductivity in the copper oxides remains elusive. Angle-resolved photoemission experiments^{1,2} revealed a kink in the dispersion relations (energy vs. wavevector) of electronic states in the cuprates at binding energies of 50-80 meV, which raises the hope that this anomaly could be key to understanding high-temperature superconductivity. This kink is often interpreted in terms of interactions between the electrons and a bosonic field. While there is no consensus on the nature of the boson or even whether a boson model is appropriate, phonons¹ and spin fluctuations² have alternatively been proposed as possible candidates for the boson model. Here we consider the role of phonons and the electron-phonon interaction in the photoemission spectra of $\text{La}_{2-x}\text{Sr}_x\text{CuO}_4$ by carrying out state-of-the-art first-principles calculations. Our study demonstrates that the phonon-induced renormalization of the electron energies and the Fermi velocity is almost one order of magnitude smaller than the effect observed in photoemission experiments. Hence, the present finding rules out electron-phonon interaction in bulk $\text{La}_{2-x}\text{Sr}_x\text{CuO}_4$ as the possible origin of the measured kink. This result should bear on several proposed theories of high temperature superconductivity in addition to theories concerning the origin of kinks in cuprate photoemission data.

During the past few years a number of high-resolution angle-resolved photoemission spectroscopy (ARPES) experiments have been performed to probe the low-energy electron or quasiparticle dynamics in cuprate superconductors³. Such studies revealed a complex interplay of many-body interactions in the cuprates by identifying several energy scales in the photoemission spectra⁴. Of particular interest and possible relevance to the theory of high-temperature superconductivity is the anomaly observed at 50-80 meV binding energies in the quasiparticle dispersions along the nodal direction of Pb-doped $\text{Bi}_2\text{Sr}_2\text{CaCu}_2\text{O}_8$, Pb-doped $\text{Bi}_2\text{Sr}_2\text{CuO}_6$, $\text{La}_{2-x}\text{Sr}_x\text{CuO}_4$ (LSCO)¹, and $\text{Bi}_2\text{Sr}_2\text{CaCu}_2\text{O}_{8+\delta}$ ², usually referred to as the “kink”. This spectral feature is currently understood as the renormalization of the quasiparticle energy resulting from an electron-boson interaction. However, no consensus has been reached so far on the nature of the collective mode involved, the principal candidates being a $q = (\pi, \pi)$ (in units of $1/a$, $a = 3.77 \text{ \AA}$ being the lattice parameter) resonant magnetic mode observed in neutron scattering⁵ and a $q = (\pi, 0)$ optical phonon corresponding to the in-plane half-breathing motion of the oxygen atoms¹. The precise nature of the kink may have important implications for the theory of cuprate superconductivity. Indeed, if the bosonic renormalization proved to be of phononic origin, the associated electron-phonon coupling - with a strength $\lambda \sim 1$ at optimal doping - would be large enough to play an important role in the pairing mechanism¹.

In this work we performed an *ab-initio* investigation of the low-energy quasiparticle renormalization due to the electron-phonon interaction in optimally doped and overdoped LSCO. We studied LSCO since it crystallizes in a simple lattice characterized by a single CuO_2 layer, and experimentally the hole concentration can be controlled over the entire phase diagram through the Sr content³. We considered optimally doped ($x = 0.15$) and heavily overdoped ($x = 0.30$) LSCO for which a mean-

field description of the electronic structure such as that given by density functional theory is appropriate to interpret measured Fermi surfaces⁶. We did not attempt to address the electron-phonon coupling in the underdoped compound since in that case the validity of the Fermi liquid paradigm has been questioned⁷. In order to calculate the electronic structure of LSCO we employed a generalized gradient approximation to density functional theory^{8,9} which correctly predicts the antiferromagnetic ground state of the parent oxide with no adjustable parameters (see Supplementary Information). Figure 1 shows the calculated Fermi surfaces of LSCO, compared with recent ARPES measurements¹⁰. The calculations are generally in good agreement with experiment, and in particular they reproduce the evolution of the Fermi surface topology from a (0, 0)-centered electron-pocket in overdoped LSCO to a (π, π) -centered hole-pocket in the underdoped compound¹¹.

We studied the lattice dynamics of LSCO by calculating the phonon eigenmodes and eigenenergies across the entire Brillouin zone through density functional perturbation theory¹². In Fig. 2 we compare the calculated phonon dispersions along the antinodal direction and the total vibrational density of states to inelastic neutron scattering data^{13,14}. The dispersion of the in-plane half-breathing Cu-O stretching mode is found to be in very good agreement with experiment. Inspection of the vibrational density of states shows that a one-to-one correspondence can be established between calculated and measured peaks, indicating an overall agreement between theory and experiment. The calculated half-breathing $(\pi, 0)$ and apical $(0, 0)$ frequencies are 68 meV and 53 meV, compared to the corresponding experimental values of 68-70 meV and 57 meV¹³, respectively. In order to extend the present comparison to the undoped parent oxide, we also performed the calculations for the $(\pi, 0)$ half-breathing mode in antiferromagnetic La_2CuO_4 . The theoretical energy of 76 meV agrees with neutron scattering measurements yielding 74

meV¹⁵, and indicates that our theoretical framework correctly describes the softening of the half-breathing phonon through the insulator-to-metal transition^{14,15}.

An electron traveling in a solid distorts the lattice due to the Coulomb interaction with the ions. The lattice distortion in turn has a feedback on the electron dynamics, resulting in an increase of the electron mass and a shortening of the electron lifetime in a particular quasiparticle state. Within quantum field theory, this effect can conveniently be described in terms of a complex self-energy Σ that the electron acquires as a consequence of the electron-phonon interaction. The real part of the self-energy describes the change in the electron energy due to this interaction, while the imaginary part provides information on the electron lifetime τ through $\tau = \hbar / (2 \text{Im} \Sigma)$. We calculated the electron self-energy within the Migdal approximation to the Feynman-Dyson perturbation theory^{16,17,18}. Due to the d -wave symmetry of the pseudogap¹⁹ and of the superconducting gap²⁰, this is a reasonable approximation for the (π, π) nodal direction. By focusing on the nodal direction we also avoid the van Hove singularity at the antinode and the comparison with experiment can be performed with little ambiguity. The diagonal part of the electron self-energy operator $\Sigma(\mathbf{r}, \mathbf{r}', \omega)$ with respect to the unperturbed electronic states arising from the electron-phonon interaction reads^{16,17,18}:

$$\begin{aligned} \Sigma_{n\mathbf{k}}(\omega) = \langle n\mathbf{k} | \Sigma(\mathbf{r}, \mathbf{r}', \omega) | n\mathbf{k} \rangle = \sum_{m\nu} \int \frac{d\mathbf{k}'}{\Omega_{\text{BZ}}} |g_{mn,\nu}(\mathbf{k}, \mathbf{k}')|^2 \times \\ \times \left[\frac{1 - f_{m\mathbf{k}'} + n_{\mathbf{q}\nu}}{\omega - \varepsilon_{m\mathbf{k}'} - \omega_{\mathbf{q}\nu} - i\delta} + \frac{f_{m\mathbf{k}'} + n_{\mathbf{q}\nu}}{\omega - \varepsilon_{m\mathbf{k}'} + \omega_{\mathbf{q}\nu} - i\delta} \right], \end{aligned} \quad (1)$$

where $|n\mathbf{k}\rangle$ indicates a Bloch eigenstate with wavevector \mathbf{k} , band index n and energy $\varepsilon_{n\mathbf{k}}$, $g_{mn,\nu}(\mathbf{k}, \mathbf{k}') = \langle m\mathbf{k}' | \Delta_{\mathbf{q}\nu} V(\mathbf{r}) | n\mathbf{k} \rangle$ is the electron-phonon matrix element for the scattering $|n\mathbf{k}\rangle \rightarrow |m\mathbf{k}'\rangle$ through a phonon of wavevector $\mathbf{q} = \mathbf{k} - \mathbf{k}'$, branch index ν and

energy $\omega_{\mathbf{q}\nu}$. The operator $\Delta_{\mathbf{q}\nu}V(\mathbf{r})$ represents the variation of the self-consistent potential with respect to a collective lattice displacement associated with this phonon, and the fermion and boson occupations $f_{m\mathbf{k}'}$ and $n_{\mathbf{q}\nu}$ account for the temperature dependence of the self-energy. The accurate evaluation of the electron self-energy requires the calculation of the electron-phonon matrix elements $g_{m\nu}(\mathbf{k},\mathbf{k}')$ on an extremely fine mesh consisting of more than a hundred thousand phonon wavevectors. This represents a formidable computational task and was beyond the reach of existing approaches. In order to overcome this difficulty we developed a new technique based on the Wannier representation²¹ which exploits the extreme short-range or nearsightedness of the electron-phonon interaction in real space^{22,23}. Figure 3 shows the electron self-energy calculated for optimally doped and overdoped LSCO at 20 K. At optimal doping the real part of the self-energy displays a peak at a binding energy of 70 meV, a shoulder at 40 meV, and a broad structure at higher binding energies around ~ 400 meV. A mode-resolved analysis shows that the main peak at 70 meV can be assigned to the Cu-O in-plane half-breathing motion around $(\pi, 0)$ and full breathing motion around (π, π) . The shoulder at 40 meV arises from phonons involving components of both out-of-plane buckling of the planar O atoms and in-plane O-O stretching vibrations. The broad feature around 400 meV can be shown to arise from a density-of-states effect. The electronic density of states displays a sharp rise at a binding energy of 400 meV, as a result of the van Hove singularity associated with the Cu d_z^2 -O2 p_z state at (π, π) . A hole with binding energy in this range has an increased probability of decaying by emitting or absorbing phonons due to the larger number of final states available. The increased decay probability appears as a peak in the imaginary part of the electron self-energy, and is reflected in the real part through a Kramers-Krönig relation due to causality (see Supplementary Discussion and Supplementary Fig. 1). As a consequence of the larger

hole concentration, in the overdoped regime the broad high-energy structure moves closer to the Fermi level and occurs at ~ 300 meV. This feature introduces an additional background to the low-energy part of the spectrum, whereby the main peak appears slightly blue-shifted and the shoulder loses intensity. Interestingly, the energy scale of 300-400 meV predicted by our calculations matches the high-energy kink recently measured²⁴ in extended range photoemission experiments on $\text{Bi}_2\text{Sr}_2\text{CaCu}_2\text{O}_{8+\delta}$ and $\text{La}_{2-x}\text{Ba}_x\text{CuO}_4$, suggesting a possible role of phonons in that context.

In order to clarify the origin of the 70 meV peak and the 40 meV shoulder we plot in Fig. 4 the squared electron-phonon matrix elements $|g(\mathbf{k}, \mathbf{k}')|^2$, which represents the transition probability from a initial $\text{Cu}d_{x^2-y^2}$ - $\text{O}p_\sigma$ nodal state with wavevector \mathbf{k} on the Fermi surface to a final state \mathbf{k}' , associated with a given phonon $\mathbf{q} = \mathbf{k}' - \mathbf{k}$. Our calculations show that the matrix elements corresponding to the half-breathing and the full breathing modes are by far the largest among all vibrational modes, thereby explaining the main peak at 70 meV in the self-energy. On the other hand, the 40 meV buckling/stretching modes show only moderately large matrix elements as compared to the 70 meV branches. However, these modes connect the nodal region with a large portion of the Fermi surface, and therefore their contribution to the self-energy is enhanced by a significant phase-space effect.

We now proceed to a quantitative comparison between our calculations and the photoemission data of ref 1. The measured peaks provide the dressed quasiparticle energy $E_{\mathbf{k}}$ for a given parallel momentum \mathbf{k} . The real part of the self-energy can be extracted from $\text{Re}\Sigma_{\mathbf{k}}(E_{\mathbf{k}}) = E_{\mathbf{k}} - \varepsilon_{\mathbf{k}}$, with $\varepsilon_{\mathbf{k}}$ the non-interacting energy¹⁷. Along the nodal direction the non-interacting dispersions are linear and we can assume $\varepsilon_{\mathbf{k}} = \mathbf{v} \cdot \mathbf{k}$ as commonly done in the literature, where the bare velocity \mathbf{v} is to be determined. We

determined the bare velocity by fitting the raw data of Figs. 1(a) and (d) of ref 1 to the simplest self-energy model consisting of a single Einstein oscillator and a constant density of states (see Supplementary Information). With the experimentally determined v , the real part of the self-energy is extracted and shown in Fig. 5. A visual comparison between the theoretical self-energy and the experimental data indicates that the effect predicted by theory is considerably weaker. In order to be quantitative and avoid ambiguity, we extracted the electron-phonon coupling strength λ by taking the low-energy slopes of both the theoretical and the experimental self-energy data sets. In particular, we took the slope at the Fermi level as an upper bound to λ , and the slope between the Fermi level and a binding energy of 50 meV as a lower bound. This procedure yielded the average electron-phonon couplings from experiment $\lambda_{\text{expt}} = 1.00-1.32$ for the optimally doped sample at 20 K, and $\lambda_{\text{expt}} = 0.75-0.99$ for the overdoped sample at 20 K, consistent with the estimates provided in ref 1. From the calculated self-energy, our analysis however yielded $\lambda_{\text{th}} = 0.14-0.22$ at optimal doping and $\lambda_{\text{th}} = 0.14-0.20$ in the overdoped regime. Hence, the calculated renormalization of the nodal Fermi velocity is $\lambda_{\text{expt}}/\lambda_{\text{th}} = 5-7$ times smaller than in experiment.

The discrepancy between theory and experiment is so large that it is unlikely to arise from any uncertainties in the calculations within our theoretical framework (see Supplementary Information) or from experiment. It is important to note that this disagreement is also found in the overdoped regime where the effects of electron correlations are reduced. These observations lead us to conclude that the electron-phonon interaction in bulk LSCO cannot account for the experimentally observed kink.

In retrospect, our results are consistent with previous first-principles calculations^{25,26} of electron-phonon interaction in the cuprates although these studies did

not address the ARPES anomaly discussed here. Brillouin zone-averaged coupling strengths $\lambda_{\text{ave}} \sim 0.4$ and $\lambda_{\text{ave}} = 0.27$ have been obtained using linear-response techniques for $\text{Ca}_{0.27}\text{Sr}_{0.63}\text{CuO}_2$ and $\text{YBa}_2\text{Cu}_3\text{O}_7$, respectively^{25,26}. When we evaluate the same parameter using the standard definition¹⁷ we obtain $\lambda_{\text{ave}} = 0.4$ for optimally doped LSCO, in agreement with those studies. In addition, a recent tight-binding study of the electron-phonon interaction in $\text{Bi}_2\text{Sr}_2\text{Ca}_{0.92}\text{Y}_{0.08}\text{Cu}_2\text{O}_{8+\delta}$ reported a spectral function in qualitative agreement with photoemission experiments²⁷. However, a close inspection of the data in Figs. 3(c2) and (c4) of ref 27 indicates a theoretical velocity renormalization of only $\lambda \sim 0.3$, in line with our calculations. Finally, a recent theoretical work²⁸ on the electron self-energy in $\text{YBa}_2\text{Cu}_3\text{O}_7$ reports an electron-phonon contribution whose magnitude is consistent with our results.

The analysis of alternative scenarios³ involving spin excitations, such as the magnetic resonance mode and the electron-magnon interaction, as well as other possible effects, is beyond the scope of the present work. However, the contribution of non-phononic mechanisms to the kink remains an important open question and calls for a thorough investigation within the framework of a quantitative theory.

In conclusion, we have presented an *ab-initio* theoretical investigation of the role of electron-phonon interaction on the low-energy photoemission spectrum of a cuprate superconductor. Our study indicates that the phonon contribution to the quasiparticle renormalization of optimally doped and overdoped LSCO is too small to take the kink observed in ARPES experiments as the signature of a strong electron-phonon interaction in bulk LSCO.

References

1. Lanzara, A. *et al.* Evidence for ubiquitous strong electron–phonon coupling in high-temperature superconductors. *Nature* **412**, 510-514 (2001).
2. Johnson, P-D. *et al.* Doping and temperature dependence of the mass enhancement observed in the cuprate $\text{Bi}_2\text{Sr}_2\text{CaCu}_2\text{O}_{8+\delta}$. *Phys. Rev. Lett.* **87**, 177007 (2001).
3. Damascelli, A., Hussain, Z. & Shen, Z-X., Angle-resolved photoemission studies of the cuprate superconductors. *Rev. Mod. Phys.* **75**, 473-541 (2003).
4. Meevasana, W. *et al.* Hierarchy of multiple many-body interaction scales in high-temperature superconductors. *Phys. Rev. B* **75**, 174506 (2007).
5. Eschrig, M. & Norman, M-R. Neutron resonance: modeling photoemission and tunneling data in the superconducting state of $\text{Bi}_2\text{Sr}_2\text{CaCu}_2\text{O}_{8+\delta}$. *Phys. Rev. Lett.* **85**, 3261-3264 (2000).
6. Sahrakorpi, S., Lindroos, M., Markiewicz, R-S. & Bansil, A. Evolution of midgap states and residual three dimensionality in $\text{La}_{2-x}\text{Sr}_x\text{CuO}_4$. *Phys. Rev. Lett.* **95**, 157601 (2005).
7. Zhou, X-J. *et al.* Dichotomy between nodal and antinodal quasiparticles in underdoped $(\text{La}_{2-x}\text{Sr}_x)\text{CuO}_4$ superconductors. *Phys. Rev. Lett.* **92**, 187001 (2004).
8. Perdew, J-P. & Wang, Y. Pair-distribution function and its coupling-constant average for the spin-polarized electron gas. *Phys. Rev. B* **46**, 12947-12954 (1992).
9. Ihm, J., Zunger, A. & Cohen, M-L. Momentum-space formalism for the total energy of solids. *J. Phys. C* **12**, 4409-4422 (1979).

10. Ino, A. *et al.* Doping-dependent evolution of the electronic structure of $\text{La}_{2-x}\text{Sr}_x\text{CuO}_4$ in the superconducting and metallic phases. *Phys. Rev. B* **65**, 094504 (2002).
11. Pickett, W-E. Electronic structure of the high-temperature oxide superconductors. *Rev. Mod. Phys.* **61**, 433-512 (1989).
12. Baroni, S., De Gironcoli, S., Dal Corso, A. & Giannozzi, P. Phonons and related crystal properties from density-functional perturbation theory. *Rev. Mod. Phys.* **73**, 515-562 (2001).
13. McQueeney, R-J. *et al.* Anomalous dispersion of LO phonons in $\text{La}_{1.85}\text{Sr}_{0.15}\text{CuO}_4$ at low temperatures. *Phys. Rev. Lett.* **82**, 628-631 (1999).
14. McQueeney, R-J., Sarrao, J-L., Pagliuso, P-G, Stephens, P-W. & Osborn, R. Mixed lattice and electronic states in high-temperature superconductors. *Phys. Rev. Lett.* **87**, 077001 (2001).
15. Pintschovius, L. *et al.* Lattice dynamical studies of HTSC materials. *Physica C* **185**, 156-151 (1991).
16. Hedin, L. & Lundqvist, S. in *Solid State Physics* Vol 15 (eds Seitz, F., Turnbull, F. & Ehrenreich, H.) 1-181 (Academic, New York, 1969).
17. Grimvall, G. *The electron-phonon interaction in metals* (North-Holland, New York, 1981).
18. Allen, P-B. & Mitrovich, B. in *Solid State Physics* Vol 37 (eds Seitz, F., Turnbull, F. & Ehrenreich, H.) 1-92 (Academic, New York, 1982).
19. Valla, T., Fedorov, A-V., Lee, J., Davis, J-C. & Gu, J-D. The ground state of the pseudogap in cuprate superconductors. *Science* **314**, 1914-1916 (2006).

20. Chen, X-K., Irwin, J-C., Trodahl, H-J., Kimura, T. & Kishio, K., Investigation of the superconducting gap in $\text{La}_{2-x}\text{Sr}_x\text{CuO}_4$ by Raman spectroscopy. *Phys. Rev. Lett.* **73**, 3290-3293 (1994).
21. Marzari, N. & Vanderbilt, D. Maximally localized generalized Wannier functions for composite energy bands. *Phys. Rev. B* **56**, 12847-12865 (1997).
22. Giustino, F., Yates, J-R., Souza, I., Cohen, M-L. & Louie, S-G. Electron-phonon interaction via electronic and lattice Wannier functions: superconductivity in boron-doped diamond reexamined. *Phys. Rev. Lett.* **98**, 047005 (2007).
23. Giustino, F., Cohen, M-L. & Louie, S-G., Electron-phonon interaction using Wannier functions. *Phys. Rev. B* **76**, 165108 (2007).
24. Valla, T. *et al.* High-energy kink observed in the electron dispersion of high-temperature cuprate superconductors. *Phys. Rev. Lett.* **98**, 167003 (2007).
25. Savrasov, S-Y. & Andersen, O-K., Linear-response calculation of the electron-phonon coupling in doped CaCuO_2 . *Phys. Rev. Lett.* **77**, 4430-4433 (1996).
26. Bohnen, K-P., Heid, R. & Krauss, M. Phonon dispersion and electron-phonon interaction for $\text{YBa}_2\text{Cu}_3\text{O}_7$ from first-principles calculations. *Europhys. Lett.* **64**, 104-110 (2003).
27. Devereaux, T-P., Cuk, T., Shen, Z-X., & Nagaosa, N. Anisotropic electron-phonon interaction in the cuprates. *Phys. Rev. Lett.* **93**, 117004 (2004).
28. Heid, R., Bohnen, K-P., Zeyher, R. & Manske, D. Momentum dependence of the electron-phonon coupling and self-energy effects in $\text{YBa}_2\text{Cu}_3\text{O}_7$ within the local density approximation. Preprint available at < <http://arxiv.org/abs/0707.4429v2>> (2007).

Acknowledgements

The authors thank Y.-W. Son and C.-H. Park for fruitful discussions. This work was supported by the National Science Foundation Grant No. DMR04-39768 and by the Director, Office of Science, Office of Basic Energy Sciences, Materials Sciences and Engineering Division, U. S. Department of Energy under Contract No. DE-AC02-05CH11231. Computational resources were provided by NPACI and NERSC. Part of the calculations were performed using the WANNIER [A. Mostofi *et al.*, www.wannier.org] and the Quantum-ESPRESSO [S. Baroni *et al.*, www.pwscf.org] packages. The Fermi surfaces were rendered using XCRYSDEN [A. Kokalj, www.xcrysden.org].

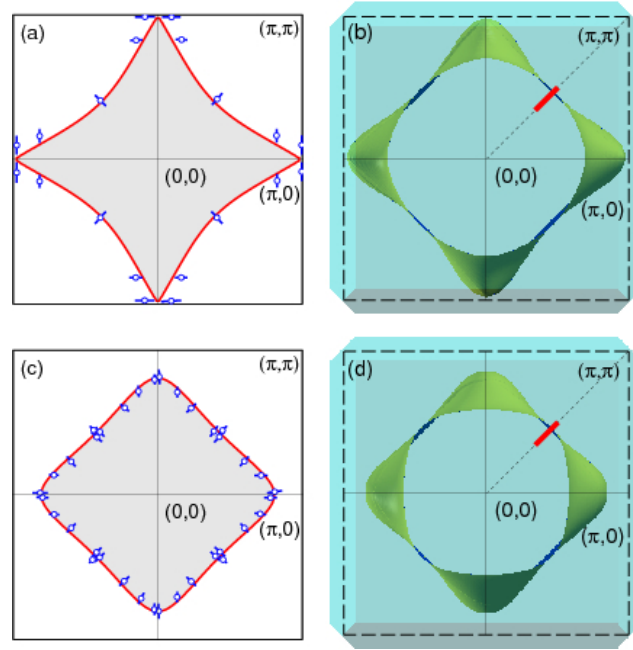


Figure 1. Fermi surfaces of $\text{La}_{2-x}\text{Sr}_x\text{CuO}_4$. Photoemission data from ref 10 for $x = 0.15$ (a), and $x = 0.30$ (c), and theoretical Fermi surfaces for $x = 0.15$ (b), and $x = 0.30$ (d). The experimental Fermi surface crossings (blue segments) correspond to the wavevectors where the leading edge of the photoemission intensity has a local maximum. The calculated Fermi surfaces in (b) and (d) are shown in a top view of the three-dimensional Brillouin zone of LSCO. The calculated nodal Fermi surface crossings $0.46 (\pi, \pi)$ and $0.44 (\pi, \pi)$ for optimally doped and overdoped LSCO compare well with the measured Fermi momenta $0.41 \pm 0.04 (\pi, \pi)$ and $0.42 \pm 0.04 (\pi, \pi)$, respectively. The comparison is less favorable for the antinodal Fermi surface crossing at optimal doping. Both the experimental and the theoretical determination of the antinodal crossing are complicated by the saddle-point van Hove singularity at $(\pi, 0)$ and the non-negligible c -axis dispersion. In (b) and (d) we show as red segments the nodal cuts along which we calculated the electron self-energy.

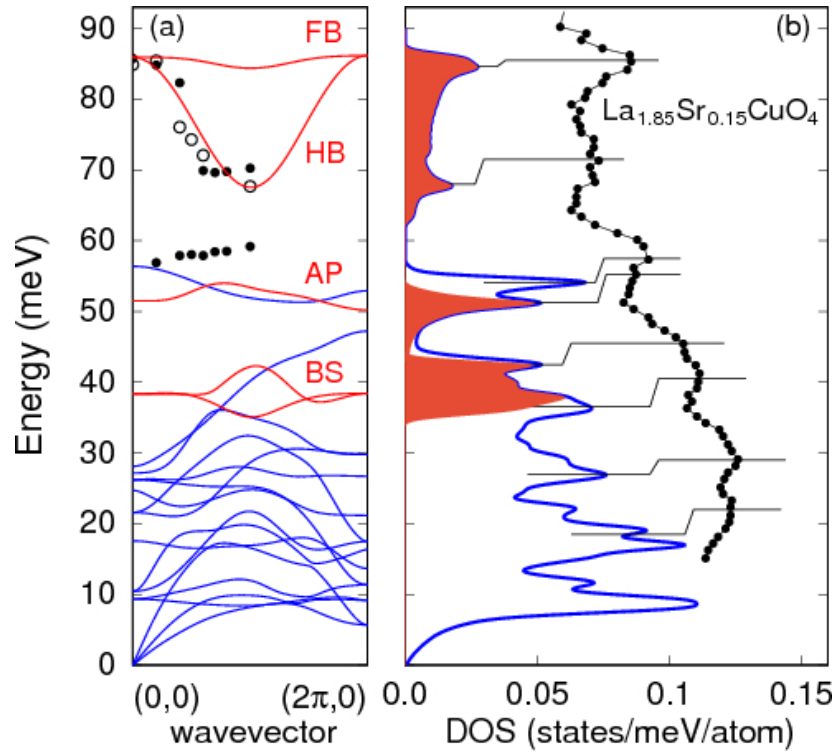


Figure 2. Phonons of $\text{La}_{2-x}\text{Sr}_x\text{CuO}_4$ at optimal doping. (a) Calculated dispersions along the antinodal direction $(0, 0)$ - $(2\pi, 0)$ (solid lines), compared to the inelastic neutron scattering data of ref 13 (circles: 300 K data, disks: 10 K data). The labels indicate the phonon branches associated with the full-breathing (FB) in-plane Cu-O stretching mode at (π, π) , to the half-breathing (HB) in-plane Cu-O stretching mode at $(\pi, 0)$, the c -axis apical (AP) O stretching mode at $(0, 0)$, and the buckling/stretching (BS) modes at $(\pi, 0)$ and (π, π) . (b) Calculated phonon density of states (solid line), compared to the inelastic neutron scattering data of ref 14 (disks). The broken lines indicate the correspondence between measured and calculated peaks. The theoretical phonon energies agree with experiment to within 5 meV.

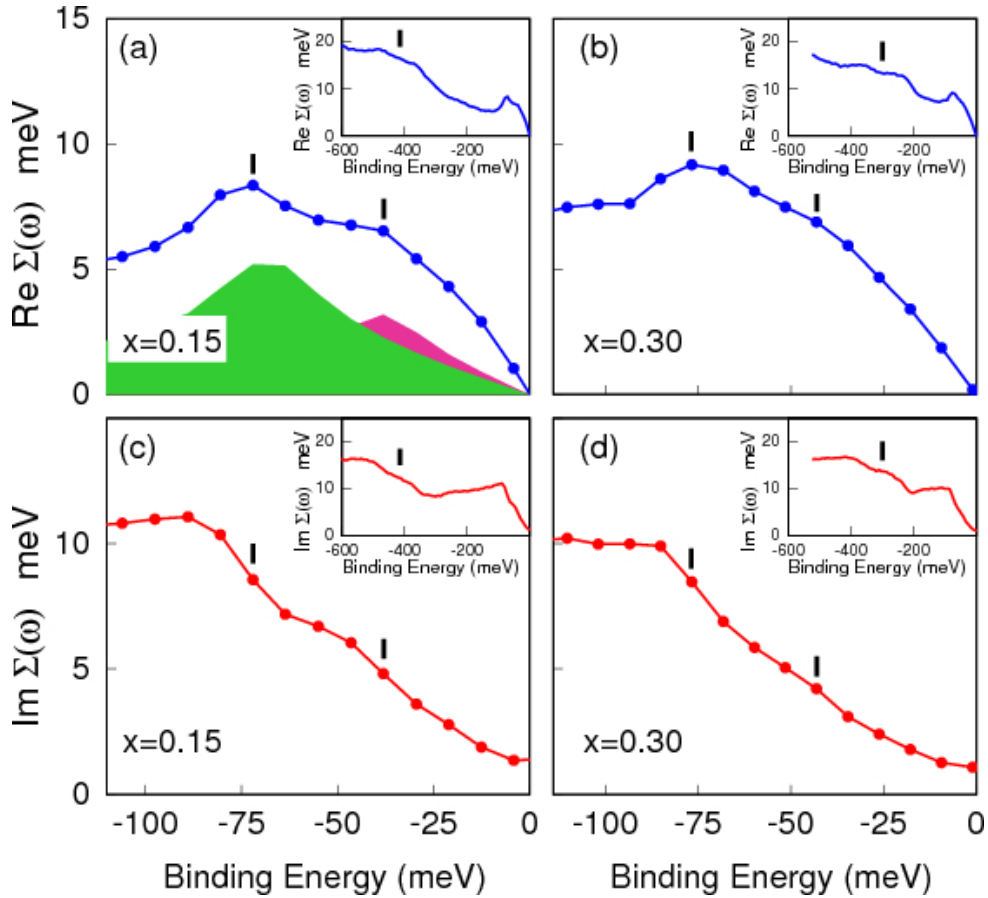


Figure 3. Calculated electron self-energy in LSCO due to the electron-phonon interaction. (a), (b) Real part of the self-energy for optimally doped ($x = 0.15$) and overdoped ($x = 0.30$) LSCO, respectively, at the temperature $T = 20$ K. (c), (d) Imaginary part of the self-energy for optimally and overdoped LSCO. Insets: real and imaginary part of the self-energy on an extended energy scale, showing the broad feature at 300-400 meV (black markers). We have computed the self-energy for electrons with the parallel momentum \mathbf{k} along the cut shown in Fig. 1(b) for three different values of the normal component k_{\perp} (0 , $\pi a/c$, and $2\pi a/c$). The variation of the self-energy along the c -axis is negligible along the cuts studied, therefore we only show the results for the cut through the zone-center. The black markers in (a) and (b) indicate the main peak at ~ 70 meV and

the shoulder at ~ 40 meV. The shaded green and purple areas represent the contributions to the self-energy from the half-breathing and full-breathing Cu-O stretching modes, and from the breathing/stretching modes around 40 meV, respectively. These contributions account for more than 80% of the real part of the self-energy. The imaginary part of the self-energy in the insets of (c) and (d) exhibits a step-like behaviour with a leading edge around 40-70 meV. This characteristic spectral shape is a consequence of Pauli's exclusion principles: holes with energy below the threshold for phonon emission $\sim 40-70$ meV cannot make transitions to above the Fermi level emitting a phonon and thus exhibit longer lifetimes.

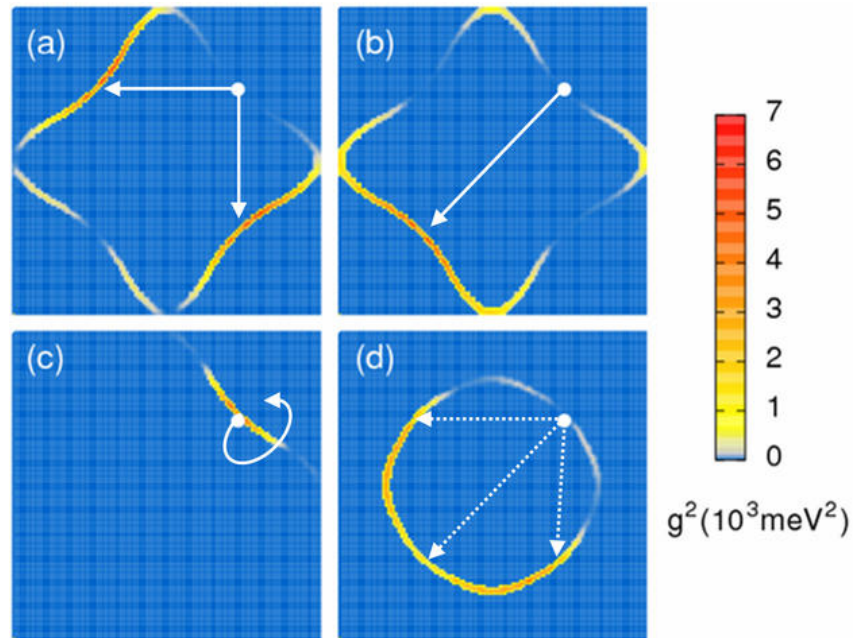


Figure 4. Electron-phonon matrix elements. Intensity plot of the squared electron-phonon matrix elements $|g(\mathbf{k}, \mathbf{k}')|^2$ giving the transition probability for the scattering from a state with \mathbf{k} on the Fermi surface (indicated by the white dot) to final states \mathbf{k}' on the Fermi surface, for optimally doped LSCO. (a) The matrix elements associated with the half-breathing phonons connect adjacent Fermi surface arcs with a maximum strength $g^2 = 7.0 \cdot 10^3 \text{ meV}^2$. (b) The full-breathing modes connect Fermi arcs on the opposite sides of the Fermi surface with a maximum strength $g^2 = 6.7 \cdot 10^3 \text{ meV}^2$. (c) The apical O stretching mode also shows large matrix elements $g^2 = 6.5 \cdot 10^3 \text{ meV}^2$. However, this phonon only gives rise to momentum-conserving transitions $\mathbf{k} = \mathbf{k}'$, hence the number of allowed final states is negligible and its coupling to nodal holes is frustrated. (d) The squared matrix element for the mixed buckling/stretching modes at 40 meV. These modes involve significant momentum transfer along the c -axis ($k'_\perp - k_\perp = 2\pi a/c$) and connect the nodal region to a large portion of the Fermi surface. The

largest matrix element in this case is $g^2 = 4.3 \cdot 10^3 \text{ meV}^2$. The squared matrix elements in overdoped LSCO are similar to those obtained at optimal doping (within 20%).

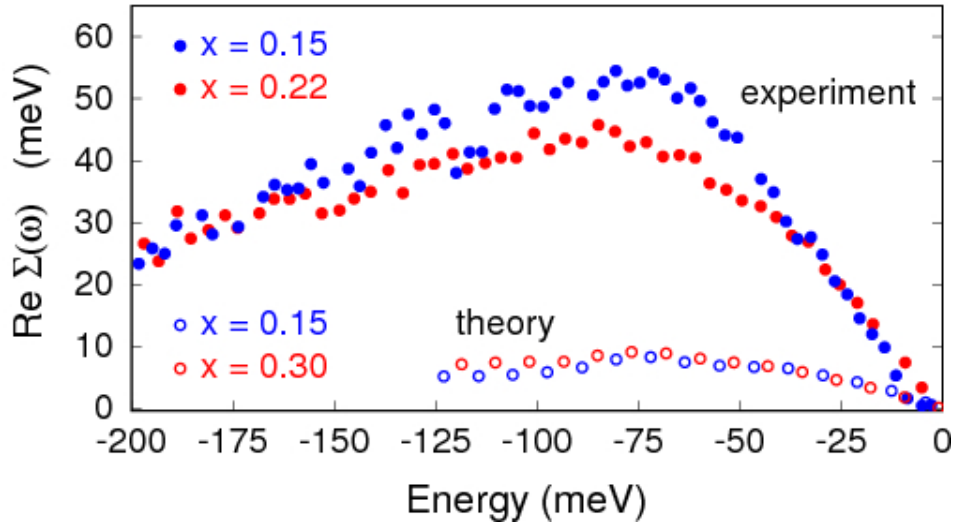


Figure 5. Comparison between theory and experiment. Comparison between the real part of the electron self-energy as obtained by ARPES experiments¹ and the first-principles theoretical self-energy arising from the electron-phonon interaction. From the raw data of Figs. 1(a) and (d) of ref 1 we extracted the self-energy assuming a linear dispersion and using a bare velocity $|v| = 4.1 \text{ eV} \cdot \text{\AA}$ obtained by a fit to the data with an Einstein electron-phonon self-energy model (see Supplementary Discussion and Supplementary Fig. 2, the precise value of the bare velocity is not critical to our conclusions). We show the experimental data at 20 K for optimally doped LSCO ($x = 0.15$) and for overdoped LSCO ($x = 0.22$), as well as the calculated self-energy at optimal doping ($x = 0.15$) and in the overdoped case ($x = 0.30$) at the same temperature.

Supplementary Information

Electron-phonon mechanism does not explain the photoemission kink in cuprate superconductors

Feliciano Giustino, Marvin L. Cohen & Steven G. Louie

Supplementary Discussion

Computational details of electronic structure and self energy

We described the electronic structure of LSCO within the generalized gradient approximation of Perdew and Wang to density functional theory¹. This functional has the advantage of correctly predicting an antiferromagnetic insulating ground state for the parent oxide La_2CuO_4 , without requiring any adjustable parameters such as in Hubbard-corrected spin-density functionals (i.e., LSDA+U). Indeed, test calculations of La_2CuO_4 in the orthorhombic structure indicate that this functional leads to a spin polarized solution with an antiferromagnetic moment of $0.58 \mu_B$, in good agreement with the experimental value² of $0.5 \mu_B$. The antiferromagnetism lifts the degeneracy between the two Cu sites and results in a small indirect band gap of 0.23 eV. This finding is consistent with previous studies indicating that, within the local spin-density approximation, La_2CuO_4 is at the edge of an antiferromagnetic phase transition³.

The valence electronic wavefunctions were expanded in a planewaves basis⁴ with a kinetic energy cutoff of 80 Ry. The core-valence interaction was taken into account by means of norm-conserving pseudopotentials of the Troullier-Martins type⁵, including the *s* and *p* semicore states for La. In all our calculations we employed the fully relaxed

tetragonal cell (space group I4/mmm) with parameters $a=3.780$ Å, $c/a=3.441$, $z_{La}/c=0.362$, $z_{O2}/c=0.184$. These parameters compare well with neutron power diffraction analysis⁶ yielding $a=3.765$ Å, $c/a=3.505$, $z_{La}/c=0.361$, $z_{O2}/c=0.183$ for $x=0.15$ and $a=3.756$ Å, $c/a=3.522$, $z_{La}/c=0.360$, $z_{O2}/c=0.181$ for $x=0.30$. Although at ambient pressure and 10 K the tetragonal-to-orthorhombic phase transition takes place at $x = 0.20$, we described optimally doped LSCO using a tetragonal cell. This is a sensible simplification since studies of LSCO under pressure showed that at 20 Kbar the structure remains tetragonal for all Sr concentrations, and at the same time the shape and magnitude of the superconducting dome is essentially identical to that measured at ambient pressure⁷. We simulated the Sr doping by removing electrons and adding a neutralizing background charge⁸.

The Wannier-Fourier interpolation^{9,10} of the electronic eigenvalues and eigenstates, the phonon energies and eigenmodes, and the electron-phonon matrix elements was performed starting from a $4\times 4\times 4$ Brillouin zone coarse mesh and checking the convergence with test calculation using an $8\times 8\times 8$ coarse mesh. In order to achieve numerical convergence, we had to include up to 128,000 inequivalent \mathbf{q} -points in the fine mesh used for the integration of the electron self-energy (Fig. 3). For the analysis of the anisotropy and strength of the electron-phonon matrix elements (Fig. 4) we adopted an even finer grid of 450,000 \mathbf{q} -points. The calculations of the electron self-energy were performed by including 17 valence bands. In terms of Wannier functions, these bands are associated with the 5 Cu- $3d$ states and the 12 O- $2p$ states. In order to check the convergence of the electron self-energy with respect to the number of electronic bands, we performed part of the calculations using an extended set of 29 bands including the 10 La $5d$ states. Overall, we considered an energy range of ± 10 eV around the Fermi level for the virtual transitions in the real part of the electron self-energy. The smearing δ in

Eq. (1) was chosen to be 1 meV, slightly larger than the accuracy of our calculated phonon energies.

The Migdal approximation to the Feynman-Dyson perturbation theory using the density functional theory band structure is reasonable for states along the nodal direction in the normal and pseudogap phases because the phonons which are responsible for the 70 meV peak in Fig. 3(a) connect only the nodal regions among themselves [Fig. 4(a) and (b)]; therefore, the important transitions contributing to the self energy are those among the un-gapped Fermi surface arcs.

We checked the convergence of the kinetic energy cutoff by repeating the calculations of the phonon dispersions with a cutoff of 120 Ry. The corresponding variation of the phonon energies was found to be negligible (0.5 meV at most).

High-energy structure in the electron self-energy

In order to show that the broad feature in the calculated self-energy around 300-400 meV in Fig. 4 arises from a density-of-states effect, we rewrite Eq. (1) by assuming a Holstein model, corresponding to an Einstein phonon spectrum peaked at the frequency Ω and a constant electron-phonon matrix element g . We also consider the zero-temperature limit for simplicity. For the imaginary part of the self-energy we find in this model:

$$\text{Im}\Sigma(\omega) = \begin{cases} \pi g^2 N(\omega - \Omega \text{sgn } \omega) & |\omega| > \Omega \\ 0 & |\omega| < \Omega \end{cases}, \quad (\text{S1})$$

N being the electronic density of states. The corresponding real part of the self-energy is found using the Kramers-Krönig relations. The self-energy calculated within this simplified model with $\Omega = 70$ meV and $g = 75$ meV is shown in Supplementary Figure 1.

The close match between the first-principles calculation and the model allows us to assign the high-energy feature to a step in the density of states of optimally doped LSCO at a binding energy of ~ 400 meV. The corresponding feature in overdoped LSCO is found at a binding energy of ~ 300 meV.

Extraction of the self-energy from experiment

We determined the noninteracting quasiparticle velocity $|\mathbf{v}|$ by fitting the raw data of Figs. 1(a) and (d) of ref 11 to the simplest self-energy model based on a single Einstein oscillator and a constant density of states¹²:

$$E_{\mathbf{k}} = \text{Re}\Sigma(E_{\mathbf{k}}) + \mathbf{v} \cdot \mathbf{k}, \quad (\text{S2})$$

$$\text{Re}\Sigma(\omega) = \frac{1}{2}\Omega\lambda \log \left| \frac{\omega + \Omega - i\Gamma}{\omega - \Omega - i\Gamma} \right|, \quad (\text{S3})$$

Besides the bare velocity, the free parameters in the fitting are the characteristic phonon energy Ω , the coupling strength λ and the broadening Γ . Such simplified model can be derived from the Holstein model of Eq. (S1) by assuming that the electronic density of states is constant and equal to the value at the Fermi level. Supplementary Figure 2 shows the self-energy determined in this way from the data of ref 11. The good quality of the fits indicates that the procedure adopted here is meaningful. This analysis gives for the model parameters the values $\Omega = 63$ meV (73 meV), $\lambda = 1.49$ (1.02), and $\Gamma = 58$ meV (37 meV) for the sample with $x = 0.15$ ($x = 0.22$) at 20 K. The bare Fermi velocity is found to be 4.05 eV $\cdot\text{\AA}$ (4.08 eV $\cdot\text{\AA}$) for the optimally doped (overdoped) sample. We note that

the precise value of the noninteracting Fermi velocity is not crucial to any of our conclusions.

Discussion of the approximations adopted

We here discuss the theoretical approximations adopted in the calculation of the self-energy.

(i) The calculations were performed within the harmonic approximation for the phonons.

It has been shown that only two phonon modes are anharmonic, the tetrahedral tilt mode and the sliding mode of the La atoms in the blocking layer¹³. These modes are soft¹⁴ around (π, π) and their contribution to the self-energy is not included in our calculations. While it cannot be excluded that such modes may increase the electron self-energy, if their contribution was significant the kink should be observed at a binding energy much smaller than 70 meV.

(ii) A Fermi-level shift and a neutralizing background were employed to account for the Sr doping. A previous calculation of $\text{La}_{2-x}\text{Sr}_x\text{CuO}_4$ taking into account the random alloying with Sr within the coherent potential approximation¹⁵ showed that the electronic structure close to the Fermi level follows a rigid-band behavior. In addition, a calculation of LaBaCuO_4 within the linearized augmented planewave method found that a rigid-band behavior describes well the electronic structure near the Fermi level¹⁶. Besides, our computed Fermi surfaces are in good agreement with the most recent measurements. All of these results justify our modeling of the Sr doping. The main drawback of the present approximation is that localization effects associated with the dopant are not taken into account. However, while hole-doping in the blocking layer (as opposed to the copper

oxide planes) has recently been suggested theoretically¹⁷, experimental evidence does not appear to support this possibility¹⁸.

(iii) *We adopted a mean-field description of the electronic structure.* While such a level of theory is not adequate in underdoped LSCO, it has been demonstrated that a good agreement is found between photoemission maps and local density calculations for optimally and overdoped LSCO when matrix element effects and three-dimensionality are taken into account¹⁹.

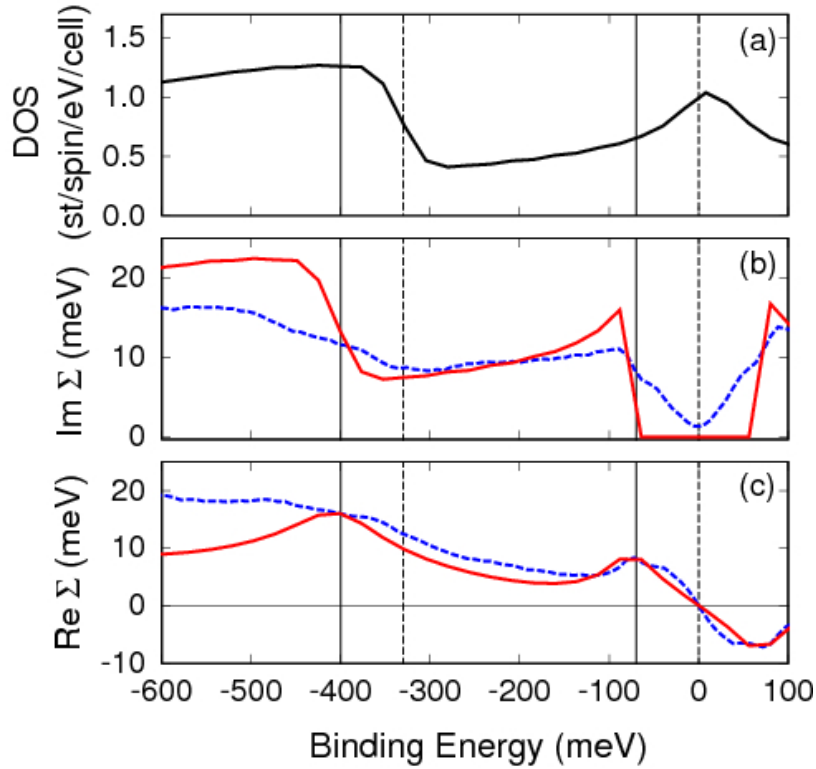
In particular, in the overdoped regime the low energy quasiparticle dispersions obtained within the local density approximation are in good agreement with recent photoemission experiments²⁰, and in overdoped LSCO our calculated self-energy is still significantly smaller than in experiment.

Supplementary References

1. Perdew, J-P. & Wang, Y. Pair-distribution function and its coupling-constant average for the spin-polarized electron gas. *Phys. Rev. B* **46**, 12947-12954 (1992).
2. Vaknin, D. *et al.* Antiferromagnetism in $\text{La}_2\text{CuO}_{4-y}$. *Phys. Rev. Lett.* **58**, 2802-2805 (1987).
3. Pickett, W-E., Electronic structure of the high-temperature oxide superconductors. *Rev. Mod. Phys.* **61**, 433-512 (1989).
4. Ihm, J., Zunger, A. & Cohen, M-L. Momentum-space formalism for the total energy of solids. *J. Phys. C* **12**, 4409-4422 (1979).
5. Troullier, N. & Martins, J-L. Efficient pseudopotentials for plane-wave calculations. *Phys. Rev. B* **43**, 1993-2006 (1991).

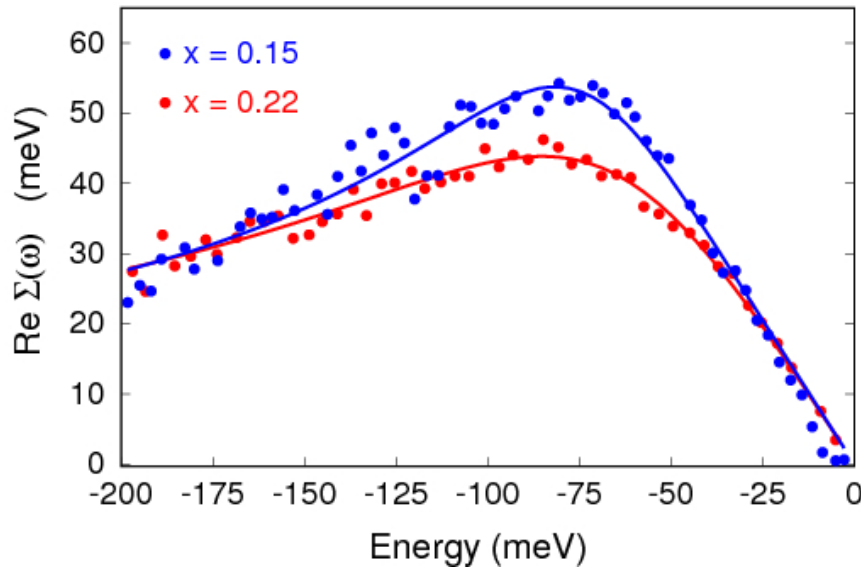
6. Radaelli, P-G. *et al.* Structural and superconducting properties of $\text{La}_{2-x}\text{Sr}_x\text{CuO}_4$ as a function of Sr content. *Phys. Rev. B* **49**, 4163-4175 (1994).
7. Yamada, N. & Ido, M. Pressure effects on superconductivity and structural phase transitions in $\text{La}_{2-x}\text{M}_x\text{CuO}_4$ ($\text{M} = \text{Ba}, \text{Sr}$). *Physica C* **203**, 240-246 (1992).
8. Savrasov, S-Y. & Andersen, O-K., Linear-response calculation of the electron-phonon coupling in doped CaCuO_2 . *Phys. Rev. Lett.* **77**, 4430-4433 (1996).
9. Giustino, F., Yates, J-R., Souza, I., Cohen, M-L. & Louie, S-G. Electron-phonon interaction via electronic and lattice Wannier functions: superconductivity in boron-doped diamond reexamined. *Phys. Rev. Lett.* **98**, 047005 (2007).
10. Giustino, F., Cohen, M-L. & Louie, S-G., Electron-phonon interaction using Wannier functions. *Phys. Rev. B* **76**, 165108 (2007).
11. Lanzara, A. *et al.* Evidence for ubiquitous strong electron-phonon coupling in high-temperature superconductors. *Nature* **412**, 510-514 (2001).
12. Grimvall, G. *The electron-phonon interaction in metals* (North-Holland, New York, 1981).
13. Cohen, R-E., Pickett, W-E. & Krakauer, H. First-principles phonon calculations for La_2CuO_4 . *Phys. Rev. Lett.* **62**, 831-834 (1989).
14. Wang, C-Z., Yu, R. & Krakauer, H. First-principles calculations of phonon dispersion and lattice dynamics in La_2CuO_4 . *Phys. Rev. B* **59**, 9278-9284 (1999).
15. Papaconstantopoulos, D-A., Pickett, W-E. & DeWeert, M-J. Calculations of the electronic structure of $\text{La}_{2-x}\text{Ba}_x\text{CuO}_{4-y}$ by the coherent-potential approximation. *Phys. Rev. Lett.* **61**, 211-214 (1988).

16. Pickett, W-E., Krakauer, H., Papaconstantopoulos, D-A. & Boyer, L-L. Evidence of conventional superconductivity in La-Ba-Cu-O compounds. *Phys. Rev. B* **35**, 7252-7255 (1987).
17. Perry, J-K., Tahir-Kheli, J. & Goddard III, W-A. *Ab initio* evidence for the formation of impurity $d_{3z^2-r^2}$ holes in doped $\text{La}_{2-x}\text{Sr}_x\text{CuO}_4$. *Phys. Rev. B* **65**, 144501 (2002).
18. Bözin, E-S. & Billinge, S-J. Nominal doping and partition of doped holes between planar and apical orbitals in $\text{La}_{2-x}\text{Sr}_x\text{CuO}_4$. *Phys. Rev. B* **72**, 174427 (2005).
19. Sahrakorpi, S., Lindroos, M., Markiewicz, R-S. & Bansil, A. Evolution of midgap states and residual three dimensionality in $\text{La}_{2-x}\text{Sr}_x\text{CuO}_4$. *Phys. Rev. Lett.* **95**, 157601 (2005).
20. Yoshida, T. *et al.* Low-energy electronic structure of the high- T_c cuprates $\text{La}_{2-x}\text{Sr}_x\text{CuO}_4$ studied by angle-resolved photoemission spectroscopy. *J. Phys.: Condens. Matter* **19**, 125209 (2007).



Supplementary Figure 1. Electron self-energy arising from the electron-phonon interaction in optimally doped LSCO. (a) Density of electronic states. The peak at the Fermi level corresponds to the saddle-point van Hove singularity of the $\text{Cu } d_{x^2-y^2} - \text{O } p_{\sigma}$ band at the antinode $(\pi, 0)$. The step at the binding energy ~ 330 meV corresponds to the local maxima of the $\text{Cu } d_{z^2} - \text{O } p_z$ band at the node (π, π) . (b) Imaginary part of the electron self-energy: *ab-initio* calculation (dashed blue line) and Holstein model [Eq. (S1), solid red line] with $\Omega = 70$ meV and $g = 75$ meV. In the Holstein model, the imaginary part of the self-energy is obtained from the density of states by “opening a gap” 2Ω at the Fermi level. As a result, the step at 330 meV in the density of states appears displaced by $\Omega = 70$ meV in the imaginary part of the self-energy. (c) Real part of the electron self-energy: *ab-initio* calculation (dashed blue line) and Holstein model [solid red line,

obtained from the imaginary part in (b) through the Kramers-Krönig relations]. The *ab-initio* self-energy appears broader than the Holstein model due to the inclusion of all phonon modes and the variation of the electron-phonon matrix element with the energy of the final electronic state.



Supplementary Figure 2. Extraction of the real part of the electron self-energy from the experimental data. Data points extracted from Fig. 1(a) of ref 11 (optimally doped LSCO at 20 K, blue disks) and Fig. 1(d) of ref 11 (overdoped LSCO at 20 K, red disks). We determined the slope of the noninteracting dispersions by fitting the raw data to the model given by Eqs. (S2) and (S3). The solid lines indicate the model self energy curves obtained with this procedure.